# OPTICA

# Mode-locked waveguide polariton laser

H. Souissi,[1] M. Gromovyi,[2,3] I. Septembre,[4] V. Develay,[1] C. Brimont,[1] L. Doyennette,[1]
E. Cambril,[2] S. Bouchoule,[2] B. Alloing,[3] E. Frayssinet,[3] J. Zúñiga-Pérez,[3,5]
T. Ackemann,[6] G. Malpuech,[4] D. D. Solnyshkov,[4,7] AND T. Guillet[1,*]

[1]*Laboratoire Charles Coulomb (L2C), Université de Montpellier, CNRS, Montpellier, France*
[2]*Centre de Nanosciences et de Nanotechnologies, CNRS, Université Paris-Saclay, Orsay, France*
[3]*UCA, CRHEA-CNRS, Rue Bernard Gregory, 06560 Valbonne, France*
[4]*Université Clermont Auvergne, CNRS, Institut Pascal, Clermont-Ferrand, France*
[5]*MajuLab, International Research Laboratory IRL 3654, CNRS, Université Côte d'Azur, Sorbonne Université, National University of Singapore, Nanyang Technological University, Singapore, Singapore*
[6]*SUPA and Department of Physics, University of Strathclyde, Glasgow G4 0NG, UK*
[7]*Institut Universitaire de France (IUF), 75231 Paris, France*
*\*thierry.guillet@umontpellier.fr*

So far, exciton-polariton (polariton) lasers were mostly single-mode lasers based on microcavities. Despite the large repulsive polariton-polariton interaction, a pulsed mode-locked polariton laser was never, to our knowledge, reported. Here, we use a 60-µm-long GaN-based waveguide surrounded by distributed Bragg reflectors forming a multi-mode horizontal cavity. We demonstrate experimentally and theoretically a polariton mode-locked micro-laser operating in the blue-UV, at room temperature, with a 300 GHz repetition rate and 100-fs-long pulses. The mode-locking is demonstrated by the compensation (linearization) of the mode dispersion by the self-phase modulation induced by the polariton-polariton interaction. It is also supported by the observation in experiment and theory of the typical envelope frequency profile of a bright soliton.

## 1. INTRODUCTION

Exciton-polaritons (polaritons) are photon modes mixed with excitons. The frequency range around the exciton frequency where this mixing is sizable is a few times the so-called Rabi splitting, which quantifies the strength of the exciton-photon interaction. Their exciton fraction confers polaritons a strongly interacting character. In the language of non-linear optics, this corresponds to a large $\chi^{(3)}$ Kerr-like non-linearity. This feature was well identified in the 2000's, when parametric amplification [1], parametric oscillation [2–5], and bistability [6,7] were observed in planar microcavities. The main difference with respect to $\chi^{(3)}$ processes in other non-linear media is that the resonant processes associated with polaritons are several orders of magnitude more efficient.

These results were obtained in GaAs-based microcavities, where the Rabi splitting is typically 10 meV resulting in a relatively narrow bandwidth detrimental to mode-locking, and where excitons are only stable at very low temperatures. A first approach to move to room temperature polaritonic devices has been based on the use of large band gap semiconductors, namely, GaN and ZnO, for which room temperature polariton lasing has been first proposed [8,9] and then observed [10–13]. The development of room-temperature polaritonics has been widened thanks to the use of organics [14,15] and, more recently, of perovskites [16–20]

and transition metal dichalcogenides (TMDs) [21]. However, the smaller exciton Bohr radius and, in most structures, the use of a bulk active medium instead of quantum wells makes the non-linear response in GaN and ZnO weaker than in equivalent GaAs structures. Thus non-linear effects have not been straightforwardly observed in these materials. In parallel to the developments in vertical microcavities, and starting from the middle of the 2010's, the study of polariton waveguides and polariton photonic crystal slabs has gained a lot of interest due to the expected benefits in terms of polariton propagation speeds, polariton lifetimes, and ease of fabrication [22,23]. Using GaAs polariton waveguides and resonant excitation [24], evidence for bright soliton creation was reported [25], and explained by the combination of repulsive polariton-polariton interactions and a positive group velocity dispersion: the associated non-linearity is two orders of magnitude larger than in other standard nonlinear media (for instance, SiN). In large band gap semiconductor waveguides, polariton lasing was predicted [26] and observed recently both in ZnO [27] and GaN [28] horizontal cavities. These in-plane cavities were several tens of micrometers long, opening up the potential for mode-locking via four-wave mixing processes. Indeed, a weak signature of non-linear polariton-polariton interaction under

non-resonant optical pumping was reported in a waveguide containing GaN-quantum wells as an active medium [29].

In Fabry–Perot cavities, photonic modes are equally spaced in frequency only if the material is non-dispersive, i.e., if it has a constant group index. However, when a dispersive Kerr-medium fills the cavity, non-linearities renormalize the eigenmode frequencies by an effect called self-phase modulation [30,31] in optics. As a matter of fact, indication for self-phase modulation in a GaN-based planar waveguide has been observed under pulsed resonant excitation [32]. Under these conditions, scattering processes involving two particles at energy $E$ and giving rise to particles at energies $E + \Delta E$ and $E - \Delta E$ become phase-matched and, thus, allowed, leading, for example, to the well-studied parametric oscillation in polariton microcavities [3,4] and polariton waveguides [23]. So-called mode-locking can occur where instead of a monomode CW laser a bright temporal soliton, with equally spaced frequency components, forms and propagates back and forth in the cavity. This dynamic behavior results in a pulsed laser output [33–35]. Mode-locking exploiting the polaritonic non-linearity has been suggested or explicitly predicted [27,29,32,36] but it has never been observed so far.

Regarding alternative near-ultraviolet and visible (NUV-VIS) mode-locked lasers, most realizations are presently based on fiber-based systems or frequency conversion. The only demonstrations based on semiconductor laser diodes rely on an external cavity [37] or a saturable absorber in a multi-section device [38] (see Ref. [39] for a review). More generally, chip-scale advanced NUV-VIS lasers based on the feedback of an absorber or an external resonator mostly rely on the heterogeneous integration of a nitride laser diode and a dielectric photonic resonator [40,41], presently limiting the advances of nitride-based photonic integrated circuits.

In this work we investigate waveguide polariton lasers based on a GaN ridge waveguide surrounded by in-plane distributed Bragg reflectors, which define horizontal Fabry–Perot resonators. In the 60-μm-long cavity, we resolve Fabry–Perot modes and determine thereby the corresponding exciton-polariton dispersion. At low temperature (70 K) monomode polariton lasing is observed. At higher temperature (from 150 K to room temperature), where polariton relaxation is enhanced, lasing takes place at lower energy and becomes intrinsically multimode. The renormalization of the eigenenergies gives rise to equally spaced mode frequencies, which is clear evidence of the buildup of resonant parametric processes where non-linear interactions produce self-phase modulation compensating for the polariton group velocity dispersion. We find a polariton mediated Kerr non-linear index $n_2 \approx 5 \times 10^{-13}$ cm$^2$ W$^{-1}$, orders of magnitude larger than non-linearity based on other mechanisms in semiconductors and in full agreement with theoretical expectations based on the magnitude of the polariton-polariton interactions. The envelope of the lasing modes is well fitted by a bright soliton wave function. This picture is confirmed by numerical simulations using the modified Gross–Pitaevskii equation and considering the precise geometry of our cavity. We thus demonstrate the first pulsed polariton laser displaying mode-locking and exploit, unambiguously, polariton non-linearities in large band gap semiconductors. Furthermore, our pulsed polariton laser operates up to room temperature and is based on a compact chip-scale device compatible with electrical injection and photonic integration, promising exploitation in integrated NUV-VIS photonics.

## 2. RESULTS

### A. Sample Design

Two similar samples are investigated in this work. The epilayer heterostructure (sample A) consists of a 3-μm-thick GaN buffer, a 1.5-μm-thick Al$_{0.08}$Ga$_{0.92}$N cladding, and a 150-nm-thick GaN waveguide core grown by metal-organic vapor phase epitaxy (MOVPE) on c-plane sapphire; the sample B differs by an additional Al$_{0.08}$Ga$_{0.92}$N cap layer of 20 nm intended to improve the carrier confinement at room temperature (Supplement 1, Section 7, Fig. S4). The planar slab waveguide is then patterned by electron beam lithography and dry deep etching, as described in Ref. [28] and shown in Figs. 1(a) and 1(b). The laser devices consist of 1-μm-wide ridge waveguides ended by four pairs of in-plane distributed Bragg reflectors (GaN-air DBRs). This work focuses on a device with a cavity length $L_{cav} = 60$ μm.

### B. Linear Regime: Polariton Dispersion below Threshold

The in-plane cavities are optically pumped with a ns-pulsed laser (355 nm, 4 ns pulses; see Supplement 1, Section 1 for additional details) that excites resonantly the exciton reservoir, as sketched in Fig. 2(a). The line-shaped pump profile (Fig. 1) is adjusted to excite partially, or entirely, the cavity length (pump length $L_{pump}$), controlling thereby the size of the exciton reservoir. These excitons in the reservoir relax and feed the lower polariton branch (LPB). The polariton dispersion evidences the strong exciton-photon coupling regime through the anti-crossing of the LPB and the exciton resonance [Fig. 2(a)], as measured and modelled in similar planar waveguides in Ref. [42]. Within the cavity, the LPB is quantized into Fabry–Perot modes with discrete wavevectors, whose signal is partially redirected to the vertical direction by the DBRs, which act not only as in-plane mirrors but also as outcouplers. This signal can be collected by the microscope objective of a micro-photoluminescence set-up. Figure 2(c) illustrates the emission spectrum of a 60-μm-long cavity in linear scale. The measurement was performed at a temperature of 150 K with a power level significantly below threshold. The spectrum displays Fabry–Perot modes from 3.380 to 3.435 eV.

The strong coupling regime between photons and excitons is assessed through the modeling of the measured cavity free spectral range (FSR), which is proportional to the first derivative of the polariton energy dispersion ($E_{LPB}$), i.e., to the group velocity $v_g$ [see Supplement 1, Section 2, Eq. (S2)]. Figure 2(d) shows a good quantitative agreement when considering the strong-coupling between the photonic TE0 mode and the GaN excitons, following the procedure detailed in Refs. [27,28]. The decrease of the FSR



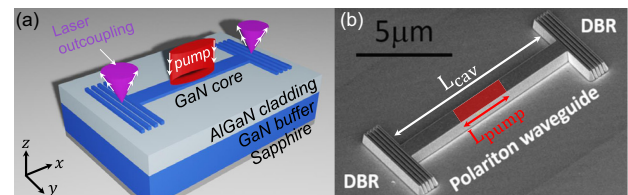**Fig. 1.** Sample description. (a) Sample structure: ridge cavity after lithography and deep etching. The guided mode propagates along the *x*-axis in the GaN core. (b) Scanning electron micrograph (SEM) image of a 10-μm-long polariton ridge waveguide in sample A. A 10-μm-long device is shown instead of the experimentally used 60-μm-long device to have enough resolution to resolve the Bragg mirror structure.
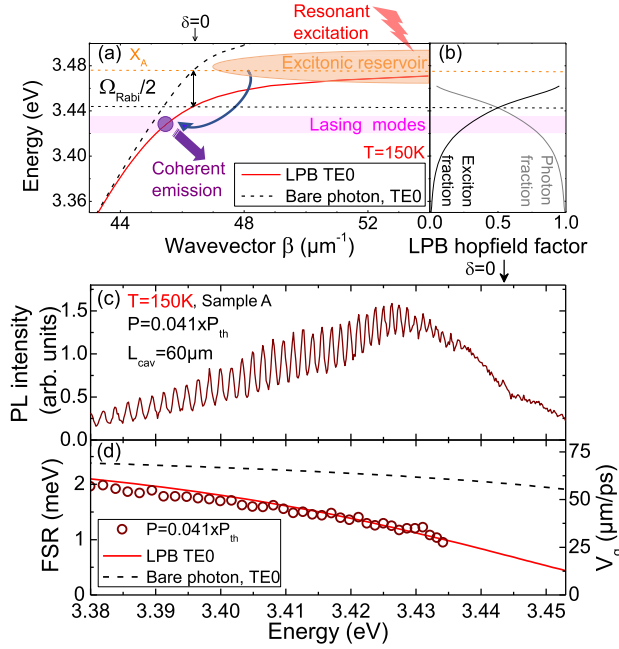
**Fig. 2.** (a) Waveguide polariton dispersion and scheme of the mechanisms involved in the polaritonic lasing. (b) Excitonic and photonic Hopfield coefficients of the LPB. (c) Emission spectrum of a 60-μm-long cavity collected at power $P = 0.041 \times P_{th}$ taken at 150 K in sample A. (d) Experimental FSR (dots) and calculated FSR from LPB dispersion (solid red line) and from the dispersion of the bare photon without excitons (dashed black line), for the TE0 mode of a planar waveguide.

from 2.0 to 0.9 meV (55% change) is reproduced by the polariton dispersion (solid red line), exhibiting a strong group velocity dispersion (GVD; see Supplement 1, Section 2). On the other hand, the FSR calculated without exciton resonances in the dielectric function ("TE0 bare photon", dashed black lines) is almost constant around 2.2 meV varying by only 12% in the same energy range. In the model the GaN exciton energy $E_{XA} = 3.475$ eV is determined from the reflectivity spectra of the same active layer taken at 150 K, whereas the core and cladding thicknesses are measured from scanning electron micrographs. At zero exciton-photon detuning ($\delta = 0$), this model provides a precise estimate of the Rabi splitting, $\Omega_{Rabi} = 64 \pm 10$ meV, characterizing the exciton-photon coupling strength, as shown in Fig. 2(a).

## C. Non-linear Regime at 70 K: Single-Mode Polariton Laser Operation

In a waveguide polariton laser, lasing occurs as soon as the population of one of the Fabry–Perot cavity modes overcomes unity so that bosonic stimulation enhances the scattering processes towards the lasing mode. Polariton laser operation in a continuous wave (CW) regime has been demonstrated for the investigated devices in Ref. [28], where they were modelled in detail. It was notably shown that polariton lasing could be achieved by pumping the entire laser cavity, as in a standard edge-emitting laser, but also when pumping only a fraction of the total length, which can be much smaller than 50% of the cavity length. This establishes a clear distinction between waveguide polariton lasers and edge-emitting lasers based on an electron-hole plasma. Furthermore, it was shown that when the pump length $L_{pump}$ amounts to only 15% of the cavity length, the polariton laser threshold shows just a three-fold increase compared to pumping the whole cavity.
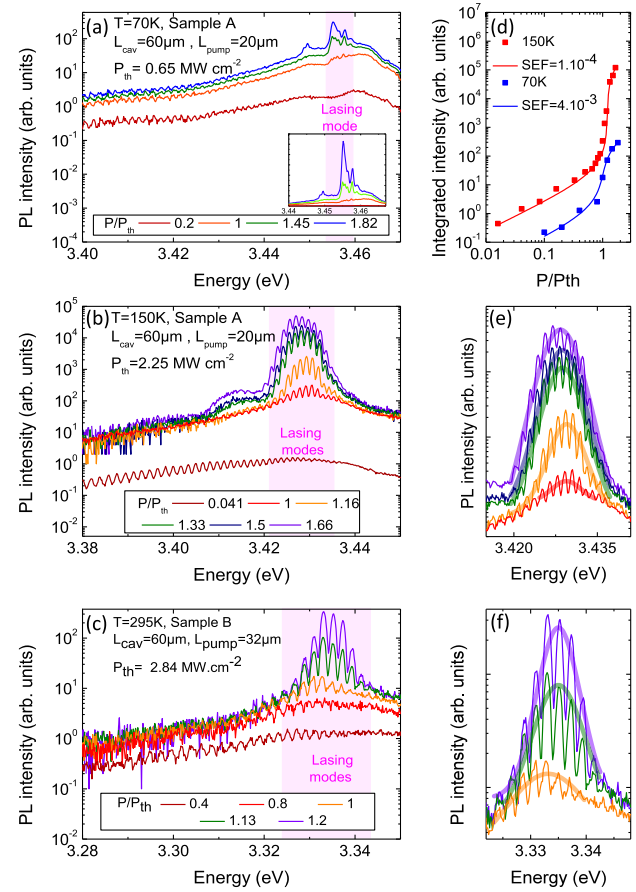


**Fig. 3.** Polariton laser operation of a 60-μm-long cavity. Power-dependent emission spectra across the lasing threshold, at (a) T = 70 K (inset shows the intensity blow-up across the lasing threshold in linear scale), (b) T = 150 K, and (c) T = 295 K. (d) Corresponding peak integrated intensity (square dots) and modelling of the spontaneous emission factor SEF (solid line) at T = 70 K (in blue) and T = 150 K (in red). (e), (f) Fit by a squared hyperbolic secant lineshape [thick light-colored plain lines, corresponding to Eq. (S8)] of the envelope of the emission spectrum above threshold (thin plain lines).

Figure 3(a) presents the CW laser operation measured at T = 70 K, which is very similar to the one reported in Ref. [28]: the spectrally resolved emission below threshold shows a set of Fabry–Perot modes covering a wide spectral range. Upon increasing the pumping intensity, some modes around 3.458 eV [close to zero exciton-photon detuning ($\delta \approx 0$)] undergo a strong non-linear intensity increase and a line narrowing, indicating quasi-single-mode CW lasing that rapidly extends to a few modes [43]. Single-mode CW lasing for a shorter pump length ($L_{pump} = 6.5$ μm) is presented in the Supplement 1, Section 5 (Fig. S1) for exactly the same cavity.

## D. Non-linear Regime from 150 K to Room Temperature: Multimode Polariton Laser Operation with Mode Synchronization

As the sample temperature is increased to T = 150 K or above, in particular at room temperature [Figs. 3(b) and 3(c)], the spectrum is almost unchanged below threshold. However, for the same pump length as in Section 2.C, the threshold value is 3.5 times and 4.5 times larger than at 70 K, respectively. The behavior at threshold is radically different since the emission is inherently multimode, with

a well-defined envelope nicely reproduced by a secant hyperbolic function [Figs. 3(e) and 3(f)] (see Supplement 1, Section 4), and about 10 modes involved in the non-linear emission. The Hopfield coefficients of the lasing modes are about 25% excitonic and 75% photonic [Fig. 2(b)] at T = 150 K and become more photonic at T = 295 K (10% excitonic, 90% photonic). The input-output characteristics [Fig. 3(d)] show that the non-linear increase of the emitted intensity is much steeper at T = 150 K (multimode case) than at T = 70 K (monomode case), with a spontaneous emission factor SEF decreasing by a factor 40, from $4 \times 10^{-3}$ to $1 \times 10^{-4}$.

The change of the waveguide polariton dispersion at threshold provides a detailed insight into the phase synchronization of the laser modes. We therefore analyze the energy shift of each cavity mode across threshold [Fig. S3(b) in Supplement 1] and the corresponding cavity FSR [Fig. 4(a)]. The spectra at T = 150 K are chosen for this detailed analysis since they present the largest mode contrast and the broadest series of modes for a largest pump power range. The same analysis at T = 295 K is provided in Supplement 1, Section 7 (Fig. S5).

Beyond threshold, it is noteworthy that the FSR of the lasing modes around 3.43 eV becomes constant [Fig. 4(a)], indicating that these modes now propagate at a common group velocity (right axis). The number of modes with a constant FSR increases from six modes at lasing threshold $P_{th}$, to 10 modes at $P = 1.66 \times P_{th}$ [Fig. 4(c)]. A more detailed sweep in terms of pumping intensities can be found in Fig. S2 in Supplement 1. The corresponding linearization of the polariton dispersion, deduced from the measured energy shift of each lasing mode, is shown in Fig. 4(b) [bare data in Figs. S3(a), (b) in Supplement 1]. The data are directly deduced from Fig. S3(b) by attributing the value $\beta_0 = 45.3\ \mu m^{-1}$ to the central lasing mode at 3.423 eV, in accordance with the theoretical dispersion far below threshold, and then adding multiples of $\pm \pi / L_{cav}$ to $\beta_0$, as imposed by the wavevector quantization in the cavity.

In semiconductor edge-emitting lasers operating in the weak coupling regime, the linearization is usually interpreted in terms of mode-locking, which occurs when the group velocity dispersion parameter $\beta_2$ and the non-linear refractive index $n_2$ (defined in Supplement 1, Sections 2 and 3) have opposite signs and the self-focusing condition is fulfilled [31]. In exciton-polariton systems, the non-linear refractive index is linked with a well-defined microscopic mechanism: polariton-polariton interactions. Meanwhile, the modification of the dispersion is interpreted in terms of the elementary excitations of the polariton fluid, at the heart of parametric processes [2,44] and superfluidity [45,46].

The spectral linewidth of the pulses [Fig. 3(e)] increases with the pumping power beyond the laser threshold, and the corresponding duration of the pulses $T_0$ decreases from 110 fs to 90 fs [Fig. 4(c)]. The pulse width at half maximum $T_{FWHM}$ [see Supplement 1, Section 4, Eq. (S7)] is about 17 times smaller than the period between pulses (3 ps for $L_{cav} = 60\ \mu m$ and $v_g \approx 40\ \mu m \cdot ps^{-1}$).

Note that the waveguide polariton lasers discussed so far in this work were achieved by pumping just a fraction of the cavity length, similar to our previous CW operation demonstration [28]. One can wonder what role is actually played by the unpumped section of the cavity. Supplement 1, Fig. S6 presents the spectra of the same device discussed above but pumped along almost the full cavity length ($L_{pump}/L_{cav} = 0.83$ instead of 0.33). The effect on the laser threshold is very similar to the one reported under
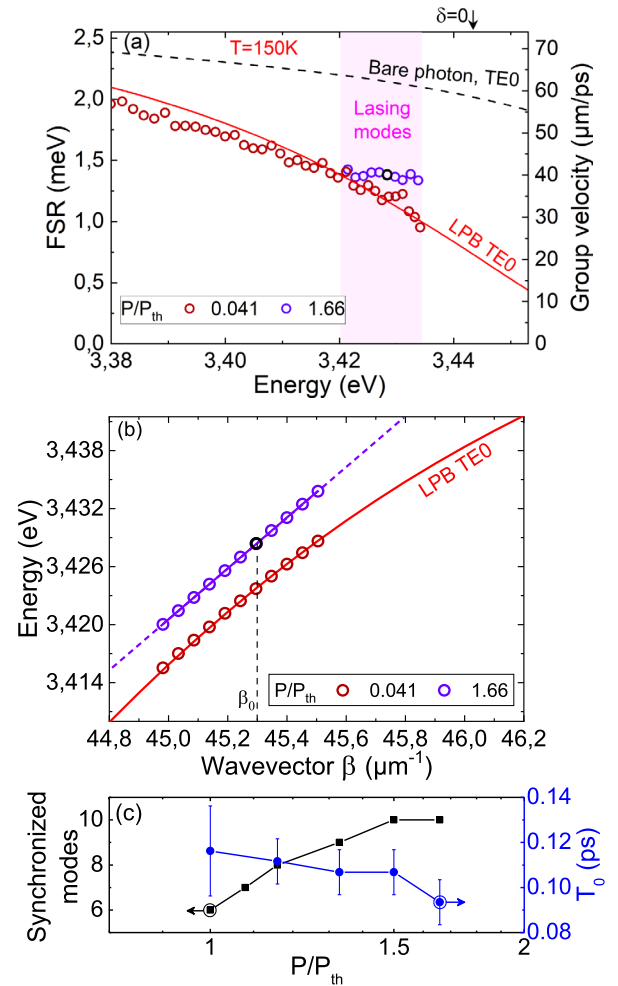


**Fig. 4.** Free spectral range (FSR) and group velocity $v_g$ of the modes across the lasing threshold for the sample A, at (a) T = 150 K and the (b) corresponding evolution of the waveguide polariton dispersion calculated for the TE0 mode of the planar waveguide. Polariton dispersions below and above threshold (respectively, red and violet). The calculated dispersion for the TE0 mode is shown as lines; the circles correspond to the longitudinal modes quantized in the 60-μm-long Fabry–Perot cavity. The black open circle indicates the central lasing mode at wavevector $\beta_0$. The dispersion beyond threshold (violet) is linear, and extended with a dotted line as a guide for the eye. (c) Number of synchronized modes and temporal pulse width $T_0$ deduced from the secant hyperbolic fit of the spectra envelope.

CW operation conditions [28]: when increasing the length of the pumping spot by a factor 2.5, the threshold pump power density decreases by a factor 3. The threshold pump energy per pulse, integrated over the pumped section, increases only by 20%, from 1.5 nJ/pulse to 1.8 nJ/pulse. This attests to the small impact of the potential additional losses associated with a large unpumped section in the cavity, which would have been totally detrimental in an edge-emitting laser operating in the weak coupling regime. Interestingly, the mode-locking dynamics is independent of the pump length: it is characterized by the same lasing energy, the same multimode emission with a hyperbolic secant spectral lineshape, and thus the same deduced pulse widths $T_0$. This demonstrates that the unpumped section of the cavity does not act as a saturable absorber.

## E.  Simulation of Polariton Mode-Locking Dynamics

In order to understand the lasing regimes observed in the experimental results, we simulate the laser dynamics inside the waveguide cavities thanks to the temporal resolution of the 1D Gross–Pitaevskii equation (GPE) for coupled excitons and photons, which is closely related to the non-linear Schrödinger equation describing mode-locking in lasers. In general, theoretical modelling of the coupled condensate-reservoir system always needs to focus on the detailed description of one of the subsystems: the condensate or the reservoir. This is due to the opposite nature of the two: the condensate is fully coherent (well-described with the Gross–Pitaevskii equation), and the reservoir is fully incoherent (well-described with the Boltzmann equations). The choice depends on what is more important in the particular problem: the dynamics of the condensate [47,48] (in which case the reservoir needs to be simplified) or the dynamics of the reservoir [26,28,29] (in which case the condensate coherent dynamics is neglected). To describe the mode-locking due to the interactions in the condensate, we obviously need to focus on the dynamics of the condensate, therefore neglecting the reservoir. The equations, qualitatively similar to Ref. [47], read

$$i\hbar\frac{\partial\psi}{\partial t} = \hat{T}\psi + U_1\psi + \Omega_R\chi/2, \tag{1}$$

$$i\hbar\frac{\partial\chi}{\partial t} = i\gamma e^{-n_x/n_{\max}} R(x)\hat{\Gamma}\chi + \xi(x, t) + \alpha_{x,1D}|\chi|^2\chi$$

$$+ U_2\chi + E_{XA}\chi + \Omega_R\psi/2, \tag{2}$$

where $\psi$ is the photon wavefunction, $\chi$ the exciton wave function, and $\Omega_R$ the Rabi splitting value. The kinetic energy operator $\hat{T}$ encodes the 1D dispersion of the photonic guided modes and is defined as $\hat{T}\psi = F^{-1}(E(k)F(\psi))$, with $F$ being the 1D Fourier transform, $F^{-1}$ its inverse, and $E(k)$ the dispersion of the guided photonic mode. Similarly, the gain operator $\hat{\Gamma}$ is defined by $\hat{\Gamma}\chi = F^{-1}(\Gamma(k)F(\chi))$, where $\Gamma(k)$ is the gain profile, which we use as an input of the model respecting features obtained in previous works [26,28,29]. Qualitatively the gain profile shifts toward lower energy and becomes wider when increasing either the temperature or the pumping power. The coefficient $\gamma$ is a scattering rate, $n_x = L_{cav}^{-1}\int|\chi|^2 dx$ is the mean exciton density in the condensate, and $n_{\max}$ a saturation density for the mean value of the 1D density (the density can locally be larger). $\xi(x, t)$ is a weak white noise term aiming to describe spontaneous scattering processes, which are absent from the Gross–Pitaevskii equation. $U_1$ and $U_2$ are the photonic and excitonic potentials, respectively, both containing high barriers at the end of the cavities with an imaginary part representing the losses at the DBRs. The excitonic potential $U_2$ also contains a contribution of the exciton reservoir $U_R R(x)$, with a variable amplitude $U_R$, whose profile is defined by the pumping spatial distribution $R(x)$. This reservoir contribution embeds both the exciton-exciton interaction and the screening of the exciton oscillator strength. $\alpha_{X,1D}$ is the 1D exciton-exciton interaction constant (see Supplement 1, Section 3) at the heart of the $\chi^{(3)}$ polariton-polariton non-linearity.

To summarize, the adjustable parameters of the model are the gain profile $\Gamma(k)$ (in particular, its width) and the saturation density $n_{\max}$. All other quantities (including the center of the gain profile) are extracted from the experiment or calculated from first principles. The simulation is performed by solving the Eqs. (1) and (2) over time with zero initial condition, until the system settles in a quasistationary regime (cf. Supplement 1, Section 8 for additional details).

For a narrow gain profile (2 meV wide) centered at polariton states corresponding to a detuning $\delta = -5$ meV and weak interactions $\alpha_{x,1D}n_{\max} \approx 0.003$ meV, the model predicts a stationary monomode lasing regime in agreement with experimental observations made at 70 K and in Ref. [28]. To describe data taken at 150 K, we use a gain centered at detuning $\delta = -20$ meV, $\alpha_{x,1D}n_{\max} \approx 0.02$ meV and we adjust the gain width to reproduce the experiment. Figure 5(a) shows the results of this simulation for a gain width of 6 meV, for which a single bright temporal soliton forms in the cavity, with a roundtrip period of 3.05 ps.

Figure 5(b) shows the Fourier transform of the temporal evolution of the soliton over a time window of 3 ns taken at one edge of the waveguide. It is compared with the experimentally measured output spectrum at $P = 1.33 \times P_{th}$. The spacing between peaks in theory is almost constant and equal to 1.35 meV for all the 10 modes shown in the figure, in good agreement with the experiment. On the other hand, the frequency width of the envelope is smaller by about 20% in theory. The theoretical spectrum can be made broader using a wider gain. However, this leads to the development of several temporal solitons competing within the cavity and the spectrum becomes less regular. We cannot conclude currently if this is a feature of the simplified model we use (we neglect the decoherence and energy relaxation within the polariton modes, for example), or if this multi-soliton regime is also present in the experiment. The experimental spectrum seems very regular and is well fitted by a sech$^2$ function, which tends to suggest a single-soliton regime. The simulation in Fig. 5 can be compared to the sech$^2$ profile both in time and in frequency, leading to a time-bandwidth product equal to 0.43; this value slightly exceeds the 0.315 lower limit expected for Fourier-transform sech$^2$ pulses, indicating that a small contribution of chirping exists in the simulated pulses.

Figure 6 shows in solid line, for the same gain width used to simulate Fig. 5, the theoretically computed FSR for increasing values of pumping (represented by $n_{\max}$ in the model). It is compared to the experimentally extracted FSR for pumping values ranging between $0.83 \times P_{th}$ and $1.66 \times P_{th}$. Below threshold, the experimental FSR (brown dotted-dashed line) varies from 1.55 meV to 1.15 meV in this frequency range (20% change), which is also the case in theory, thus confirming that the experimental and theoretical energy dispersion relations are in good agreement. Increasing pumping, the FSR of modes at lower energy decreases from 1.55 to 1.35 meV, whereas the FSR of modes at higher energy increases from 1.15 to 1.35 meV. The FSR of central modes stays constant. At the highest pumping value the FSR of the 10 modes involved in the soliton becomes constant in energy at 1.35–1.36 meV, within an accuracy of 2%, which is a very clear signature of a mode-locking effect. The theoretical calculation reproduces this effect completely. The trajectory of individual FSR is well described, including the fact that FSR does not evolve monotonically versus pumping: FSR can slightly increase first and then decrease towards 1.35 meV, or vice versa.

These observations clearly confirm the possibility of mode-locking and self-pulsing via polaritonic non-linearities as suggested in earlier works on polariton amplification in ZnO and GaN polariton waveguides [27,29,32,49], and in theoretical proposals
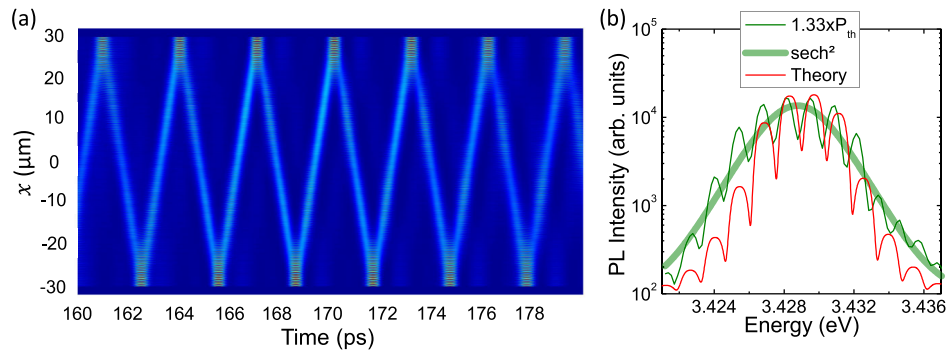
**Fig. 5.** (a) Simulation of the time- and spatially resolved polariton population after the start of a continuous pumping of the exciton reservoir at $t = 0$ (for $\alpha n_{max} = 0.02$ meV); $L_{cav} = 60\ \mu m$, $L_{pump} = 20\ \mu m$, T = 150 K. (b) Comparison between the output spectra measured at $P = 1.33 \times P_{th}$ [thin green line (sample A)] and calculated (thin red line); hyperbolic secant squared fit (thick green line).
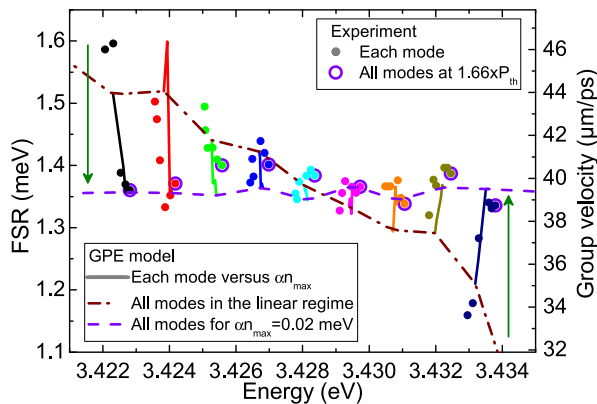


**Fig. 6.** Trajectory of each lasing mode (dots: one color per mode) in FSR-energy coordinates for different pumping powers. Data points indicate experimental results (sample A); the plain lines represent the results of the GPE model for polariton mode-locking. Theoretical trajectories of modes in the linear regime and for $\alpha n_{max} = 0.02$ meV are indicated as a dashed-dotted line and dashed line, respectively.

on frequency comb generation in polaritonic microring resonators [36], but had never been achieved.

## 3. QUANTIFICATION OF POLARITON NON-LINEARITIES

The observed mode-locking of a polariton laser exhibits distinct characteristics compared to the standard figures of merit in other non-linear optical systems (as defined in Ref. [31] and detailed in the Supplement 1).

(i) Due to the short cavity length, the roundtrip time of the pulse train (3 ps) corresponds to a repetition frequency larger than 300 GHz. A direct time-resolved observation of the pulsed regime is therefore very difficult to provide experimentally.

(ii) As shown in Fig. 4(a), the group velocity varies by more than 20% (from 40 to 26 $\mu m \cdot ps^{-1}$) within the spectral range involved in mode-locked lasing; this relates to a group velocity dispersion parameter $\beta_2 = 4 \times 10^{-22}\ s^2 \cdot m^{-1}$, which is four orders of magnitude larger than in non-linear optical fibers [50] and two orders of magnitude larger than in AlGaAs waveguides investigated for soliton formation [51]. The corresponding "dispersion length" is $L_D = T_0^2 / |\beta_2| \approx 25\ \mu m$ [31] (see Supplement 1, Section 4), one order of magnitude smaller

than the typical mm-scaled values in non-linear waveguides [51] and comparable to the cavity length in the presently investigated cavities.

(iii) The energy per pulse of the current mode-locked laser is difficult to estimate since the in-plane output of the laser devices cannot be directly accessed: indeed, only a small and unknown fraction of the laser emission is collected thanks to the scattering by the DBRs. To obtain a quantitative estimation, we here consider that the lasing mode occupancy at threshold is close to one. The integrated intensity is rising at threshold by a factor $10^4$ at T = 150 K [Fig. 3(d)]. We therefore consider that the soliton contains $N \approx 10^4$ polaritons. This corresponds to a soliton energy of 5.5 fJ, and a soliton peak power $P_0 \approx 55$ mW. Such pulse energies are two to three orders of magnitude smaller than the threshold for phase modulation reported in similar waveguides under resonant excitation (50 pJ per 100-fs-long pulse, with a five times wider transverse mode profile) [32].

This energy analysis allows estimating which fraction of the pumping laser is transferred to the soliton, which turns out to be of the order of 0.3%: indeed, each 4-ns-long pump pulse has an energy of 1.8 nJ at threshold, and generates a train of about 1000 mode-locked pulses, based on the roundtrip time. This 0.3% conversion from the optical pump to the polariton laser emission accounts for the geometrical matching between the pump spot and the 1-$\mu$m-wide ridge, for the absorption by the active layer, and for the competition between exciton spontaneous emission in the reservoir and exciton stimulated relaxation towards the polariton lasing modes.

(iv) The Kerr-type non-linearities involve the polariton-polariton interaction constant $\alpha$ (see Supplement 1, Section 3). The value deduced from the measured FSR shift (0.2 meV) through Eq. (S4) is $\alpha \approx 6.3\ 10^{-6}$ meV, quite close (just a factor 2) to the theoretical value $\alpha \approx 2.5\ 10^{-6}$ meV when considering exciton-exciton interactions in a waveguide [Eq. (S5) in Supplement 1]. One should notice that in theory the interaction energy in the soliton is 15 times larger than $\alpha_{X,1D} n_{max}$ because the $N$ polaritons present in the system are not distributed along the 60 $\mu$m of the sample, but concentrated in the 4 $\mu$m healing length of the soliton. We can thereby deduce the non-linear refractive index $n_2$, with an experimental value of $n_2 \approx 4.7 \times 10^{-13}\ cm^2 \cdot W^{-1}$ and a theoretical value just a factor 2 larger $n_2 \approx 10^{-12}\ cm^2 \cdot W^{-1}$, for a polariton-polariton $\chi^{(3)}$ non-linearity. It is three

orders of magnitude larger than in bulk non-linear materials, and three times larger than in AlGaAs waveguides [51]. Accounting for the transverse effective area of the guided modes $A_{\text{eff}}$, we can estimate the non-linear length $L_{\text{NL}} = n_0 A_{\text{eff}} / (\beta_0 |n_2| P_0) \approx 25 - 250 \, \mu\text{m}$.

The estimated value of $n_2$ is close to the estimates of Ref. [32] for QW-based nitride polariton waveguides, which are similar to ours but without Fabry–Perot cavities. Indeed, in Ref. [32] the deposited gratings are only used for the coupling of the resonant excitation laser to the waveguide polariton modes and their collection. Instead, in the present work the DBRs define an in-plane cavity providing the necessary laser feedback. Besides, they also outcouple a fraction of the laser emission to the vertical direction, enabling us to collect it. In Ref. [32] a spectral broadening of the injected 100-fs-long light pulses was observed and interpreted in terms of polariton non-linearities involving the exciton-exciton repulsion and the reduction of the exciton oscillator strength, both contributing to a density-dependent blueshift of the polariton frequency. The non-linearity was measured for freely propagating polaritons without feedback, down to propagation lengths of 100 μm and resonant pump energies of 50 pJ/pulse. Under non-resonant excitation, similar waveguides without cavity feedback also evidenced the onset of modulation instability of the polariton relaxation [29], which is additional evidence of Kerr-like parametric processes.

The present results, with both a flattening of the FSR and a hyperbolic secant spectral lineshape, provide a clear demonstration that the parametric processes foster mode synchronization among the lasing modes. We emphasize that the orders of magnitude of the non-linear length $L_{\text{NL}}$, of the dispersion length $L_D$, and of the roundtrip length $2L_{\text{cav}}$ in our cavities are comparable, which is consistent with the onset of mode-locking in our devices. This exemplifies how polariton waveguide devices are prone to reduce both the length scale and the energy scale of non-linear photonic devices, and increase the operation frequency.

## 4. CONNECTION WITH CONVENTIONAL MODE-LOCKED SEMI-CONDUCTORS AND SOLID-STATE LASERS

Passive mode-locking, i.e., mode-locking that does not demand an external modulation, is usually achieved via a saturable absorber, most often on a semiconductor basis [35], although the resulting pulse might be close to a Kerr-soliton [52–54]. Even in the case of the so-called Kerr-lens mode-locking in Ti:Saphire lasers [55] (and some vertical-cavity semiconductor lasers [56,57]), the mode-locking is primarily not a dispersive effect but achieved via saturable losses, i.e., a generalized form of saturated absorption, as the change of modal size due to non-linear lensing changes the losses at intra-cavity apertures [35]. Similarly, non-linear polarization rotation in fiber lasers controls losses in the polarization sensitive elements [58]. In edge-emitting semiconductor lasers, saturable absorption is usually provided by an unpumped absorber section and a pumped gain section in so-called two-section devices [34,59–61], which were implemented in nitride QW-based laser diodes operating in a Q-switch regime [62,63] and a mode-locked regime [38]. On the contrary, in our results the independence of the mode-locking on the fraction of pumped cavity length indicates that the polariton system does not operate as a two-sections device, in the sense described before.

There have been some observations of passive mode-locking in single-section edge-emitting lasers, in particular for quantum dash and quantum dot gain materials [64–66]. This has been sometimes referred to as "magic" mode-locking [67], in analogy to the "magic" mode-locking in Ti:Saphire lasers before the role of saturable losses at apertures in Kerr-lens mode-locking was understood [35]. There has been some debate whether mode-locking in single-section devices is due to intrinsic non-linearities as the Kerr-non-linearity from four-wave mixing only or whether unintentional saturable absorption in not sufficiently pumped perimeter areas plays a role [68]. Recent work indicates that four-wave mixing in combination with other non-linearities as gain saturation and spatial hole burning can be indeed enough to explain sustained mode-locking [61,68,69] but its quality and stability depend strongly on injection levels [68] and/or extra-cavity pulse suppression might be required for longer lasers [66]. Polaritonic systems with very strong Kerr interactions are hence expected to be more robust.

## 5. CONCLUSION

In summary, we have presented the demonstration of a pulsed polariton laser operating from T = 150 K to room temperature, and relying on a mode-locking mechanism based on the strong polariton-polariton Kerr non-linearity. This last non-linearity is strong enough to compensate for the large group velocity dispersion associated to the lower polariton branch in the strong exciton-photon coupling regime. The chosen cavity geometry, with a GaN-based active layer, is highly similar to standard ridge semiconductor edge-emitting lasers, but our investigation as a function of the gain length highlights the strong difference with the saturable absorber approach to mode-locking. This design is compatible with standard electrical schemes and with further integration into nitride-based photonic circuits targeting the NUV-VIS spectral range. The spectral signatures of mode-locking are well reproduced through simulations solving the Gross–Pitaevskii equation for the coupled exciton and photon fields, leading to 100 fs solitons. The detailed modelling at T = 150 K leads to an estimated 5 fJ soliton energy per pulse, well-suited to applications requiring low-energy laser pulses. Overall, the compact micrometric footprint, the laser repetition frequency beyond 300 GHz, and the room-temperature operation confer these polariton-based pulsed lasers promising figures of merit for the development of UV integrated photonics sources.

**Disclosures.** The authors declare no conflicts of interest.

**Data availability.** Data underlying the results presented in this paper and Supplement 1 are available in Ref. [70].

**Supplemental document.** See Supplement 1 for supporting content.

## REFERENCES

1. M. Saba, C. Ciuti, J. Bloch, *et al.*, "High-temperature ultrafast polariton parametric amplification in semiconductor microcavities," Nature **414**, 731–735 (2001).

2. P. G. Savvidis, J. J. Baumberg, R. M. Stevenson, *et al.*, "Angle-resonant stimulated polariton amplifier," Phys. Rev. Lett. **84**, 1547–1550 (2000).

3. J. J. Baumberg, P. G. Savvidis, R. M. Stevenson, *et al.*, "Parametric oscillation in a vertical microcavity: a polariton condensate or micro-optical parametric oscillation," Phys. Rev. B **62**, R16247 (2000).

4. R. M. Stevenson, V. N. Astratov, M. S. Skolnick, *et al.*, "Continuous wave observation of massive polariton redistribution by stimulated scattering in semiconductor microcavities," Phys. Rev. Lett. **85**, 3680–3683 (2000).

5. D. M. Whittaker, "Classical treatment of parametric processes in a strong-coupling planar microcavity," Phys. Rev. B **63**, 193305 (2001).

6. A. Baas, J. P. Karr, H. Eleuch, *et al.*, "Optical bistability in semiconductor microcavities," Phys. Rev. A **69**, 023809 (2004).

7. A. Baas, J.-P. Karr, M. Romanelli, *et al.*, "Optical bistability in semiconductor microcavities in the nondegenerate parametric oscillation regime: analogy with the optical parametric oscillator," Phys. Rev. B **70**, 161307 (2004).

8. G. Malpuech, A. Di Carlo, A. Kavokin, *et al.*, "Room-temperature polariton lasers based on GaN microcavities," Appl. Phys. Lett. **81**, 412–414 (2002).

9. M. Zamfirescu, A. Kavokin, B. Gil, *et al.*, "ZnO as a material mostly adapted for the realization of room-temperature polariton lasers," Phys. Rev. B **65**, 161205 (2002).

10. S. Christopoulos, G. B. H. von Högersthal, A. J. D. Grundy, *et al.*, "Room-temperature polariton lasing in semiconductor microcavities," Phys. Rev. Lett. **98**, 126405 (2007).

11. J. J. Baumberg, A. V. Kavokin, S. Christopoulos, *et al.*, "Spontaneous polarization buildup in a room-temperature polariton laser," Phys. Rev. Lett. **101**, 136409 (2008).

12. G. Christmann, R. Butté, E. Feltin, *et al.*, "Room temperature polariton lasing in a GaN/AlGaN multiple quantum well microcavity," Appl. Phys. Lett. **93**, 051102 (2008).

13. F. Li, L. Orosz, O. Kamoun, *et al.*, "From excitonic to photonic polariton condensate in a ZnO-based microcavity," Phys. Rev. Lett. **110**, 196406 (2013).

14. S. Kéna-Cohen and S. Forrest, "Room-temperature polariton lasing in an organic single-crystal microcavity," Nat. Photonics **4**, 371–375 (2010).

15. J. D. Plumhof, T. Stöferle, L. Mai, *et al.*, "Room-temperature Bose–Einstein condensation of cavity exciton–polaritons in a polymer," Nat. Mater. **13**, 247–252 (2013).

16. R. Su, J. Wang, J. Zhao, *et al.*, "Room temperature long-range coherent exciton polariton condensate flow in lead halide perovskites," Sci. Adv. **4**, eaau0244 (2018).

17. R. Su, S. Ghosh, J. Wang, *et al.*, "Observation of exciton polariton condensation in a perovskite lattice at room temperature," Nat. Phys. **16**, 301–306 (2020).

18. L. Lu, Q. Le-Van, L. Ferrier, *et al.*, "Engineering a light-matter strong coupling regime in perovskite-based plasmonic metasurface: quasi-bound state in the continuum and exceptional points," Photon. Res. **8**, A91–A100 (2020).

19. R. Tao, K. Peng, L. Haeberlé, *et al.*, "Halide perovskites enable polaritonic XY spin Hamiltonian at room temperature," Nat. Mater. **21**, 761–766 (2022).

20. K. Peng, R. Tao, L. Haeberlé, *et al.*, "Room-temperature polariton quantum fluids in halide perovskites," Nat. Commun. **13**, 7388 (2022).

21. J. Zhao, R. Su, A. Fieramosca, *et al.*, "Ultralow threshold polariton condensate in a monolayer semiconductor microcavity at room temperature," Nano Lett. **21**, 3331–3339 (2021).

22. D. Bajoni, D. Gerace, M. Galli, *et al.*, "Exciton polaritons in two-dimensional photonic crystals," Phys. Rev. B **80**, 201308 (2009).

23. D. G. Suárez-Forero, F. Riminucci, V. Ardizzone, *et al.*, "Enhancement of parametric effects in polariton waveguides induced by dipolar interactions," Phys. Rev. Lett. **126**, 137401 (2021).

24. P. M. Walker, L. Tinkler, M. Durska, *et al.*, "Exciton polaritons in semiconductor waveguides," Appl. Phys. Lett. **102**, 012109 (2013).

25. P. M. Walker, L. Tinkler, D. V. Skryabin, *et al.*, "Ultra-low-power hybrid light–matter solitons," Nat. Commun. **6**, 8317 (2015).

26. D. D. Solnyshkov, H. Terças, and G. Malpuech, "Optical amplifier based on guided polaritons in GaN and ZnO," Appl. Phys. Lett. **105**, 231102 (2014).

27. O. Jamadi, F. Reveret, P. Disseix, *et al.*, "Edge-emitting polariton laser and amplifier based on a ZnO waveguide," Light Sci. Appl. **7**, 82 (2018).

28. H. Souissi, M. Gromovyi, T. Gueye, *et al.*, "Ridge polariton laser: different from a semiconductor edge-emitting laser," Phys. Rev. Appl. **18**, 044029 (2022).

29. J. Ciers, D. D. Solnyshkov, G. Callsen, *et al.*, "Polariton relaxation and polariton nonlinearities in nonresonantly cw-pumped III-nitride slab waveguides," Phys. Rev. B **102**, 155304 (2020).

30. G. Agrawal and N. Olsson, "Self-phase modulation and spectral broadening of optical pulses in semiconductor laser amplifiers," IEEE J. Quantum Electron. **25**, 2297–2306 (1989).

31. G. P. Agrawal, *Nonlinear Fiber Optics* (Academic, 2001).

32. D. Paola, P. M. Walker, R. P. A. Emmanuele, *et al.*, "Ultrafast-nonlinear ultraviolet pulse modulation in an AlInGaN polariton waveguide operating up to room temperature," Nat. Commun. **12**, 3504 (2021).

33. M. Hofer, M. Fermann, F. Haberl, *et al.*, "Mode-locking with cross-phase and self-phase modulation," Opt. Lett. **16**, 502–504 (1991).

34. P. Vasil'ev, I. White, and J. Gowar, "Fast phenomena in semiconductor lasers," Rep. Prog. Phys. **63**, 1997–2042 (2000).

35. U. Keller, "Ultrafast solid-state laser oscillators: a success story for the last 20 years with no end in sight," Appl. Phys. B **100**, 15–28 (2010).

36. O. A. Egorov and D. V. Skryabin, "Frequency comb generation in a resonantly pumped exciton-polariton microring resonator," Opt. Express **26**, 24003–24009 (2018).

37. T. Weig, H. Höck, K. Holc, *et al.*, "Implementation and investigation of mode locking in GaN-based laser diodes in external cavity configuration," Phys. Status Solidi A **212**, 986–991 (2014).

38. P. P. Vasil'ev, A. B. Sergeev, I. V. Smetanin, *et al.*, "Mode locking in monolithic two-section InGaN blue-violet semiconductor lasers," Appl. Phys. Lett. **102**, 121115 (2013).

39. A. Hermans, K. Van Gasse, and B. Kuyken, "On-chip optical comb sources," APL Photon. **7**, 100901 (2022).

40. A. A. Savchenkov, S.-W. Chiow, M. Ghasemkhani, *et al.*, "Self-injection locking efficiency of a UV Fabry–Perot laser diode," Opt. Lett. **44**, 4175–4178 (2019).

41. T. Wunderer, A. Siddharth, N. M. Johnson, *et al.*, "Single-frequency violet and blue laser emission from AlGaInN photonic integrated circuit chips," Opt. Lett. **48**, 2781–2784 (2023).

42. C. Brimont, L. Doyennette, G. Kreyder, *et al.*, "Strong coupling of exciton-polaritons in a bulk GaN planar waveguide: quantifying the coupling strength," Phys. Rev. Appl. **14**, 054060 (2020).

43. L. Yang, G. Li, X. Gao, *et al.*, "Topological-cavity surface-emitting laser," Nat. Photonics **16**, 279–283 (2022).

44. P. G. Savvidis, J. J. Baumberg, R. M. Stevenson, *et al.*, "Asymmetric angular emission in semiconductor microcavities," Phys. Rev. B **62**, R13278 (2000).

45. S. Utsunomiya, L. Tian, G. Roumpos, *et al.*, "Observation of bogoliubov excitations in exciton-polariton condensates," Nat. Phys. **4**, 700–705 (2008).

46. A. Amo, S. Pigeon, D. Sanvitto, *et al.*, "Polariton superfluids reveal quantum hydrodynamic solitons," Science **332**, 1167–1170 (2011).

47. E. Wertz, A. Amo, D. D. Solnyshkov, *et al.*, "Propagation and amplification dynamics of 1D polariton condensates," Phys. Rev. Lett. **109**, 216404 (2012).

48. D. D. Solnyshkov, H. Terças, K. Dini, *et al.*, "Hybrid Boltzmann–Gross-Pitaevskii theory of Bose-Einstein condensation and superfluidity in open driven-dissipative systems," Phys. Rev. A **89**, 033626 (2014).

49. A. Delphan, M. N. Makhonin, T. Isoniemi, *et al.*, "Polariton lasing in AlGaN microring with GaN/AlGaN quantum wells," APL Photon. **8**, 021302 (2023).

50. J. M. Dudley, G. Genty, and S. Coen, "Supercontinuum generation in photonic crystal fiber," Rev. Mod. Phys. **78**, 1135–1184 (2006).

51. N. Bélanger, A. Villeneuve, and J. S. Aitchison, "Solitonlike pulses in self-defocusing AlGaAs waveguides," J. Opt. Soc. Am. B **14**, 3003–3012 (1997).

52. H. A. Haus, "Theory of mode locking with a slow saturable absorber," IEEE J. Quantum Electron. **11**, 736–746 (1975).

53. I. D. Jung, F. X. Kärtner, L. R. Brovelli, *et al.*, "Experimental verification of soliton mode locking using only a slow saturable absorber," Opt. Lett. **20**, 1892–1894 (1995).

54. R. Paschotta, R. Häring, A. Garnache, *et al.*, "Soliton-like pulse-shaping mechanism in passively mode-locked surface-emitting semiconductor lasers," Appl. Phys. B **75**, 445–451 (2002).

55. D. E. Spence, P. N. Kean, and W. Sibbett, "60-fsec pulse generation from a self-mode locked Ti-sapphire laser," Opt. Lett. **16**, 42–45 (1991).

56. L. Kornaszewski, G. Maker, G. P. A. Malcolm, *et al.*, "SESAM-free mode-locked semiconductor disk laser," Laser Photon. Rev. **6**, L20–L23 (2012).

57. A. R. Albrecht, Y. Wang, M. Ghasemkhani, *et al.*, "Exploring ultra-fast negative Kerr effect for mode-locking vertical external-cavity surface-emitting lasers," Opt. Express **21**, 28801–28808 (2013).

58. V. J. Matsas, T. P. Newson, D. J. Richardson, *et al.*, "Selfstarting passively mode-locked fibre ring soliton laser exploiting nonlinear polarisation rotation," Electron. Lett. **28**, 1391–1393 (1992).

59. J. H. Marsh, "Mode-locked laser diodes and their monolithic integration," IEEE J. Sel. Top. Quantum Electron. **23**, 1100611 (2017).

60. W. Wei, J. Chen, J. Huang, *et al.*, "Advances of semiconductor mode-locked laser for optical frequency comb generation," Natl. Sci. Open **1**, 20220026 (2022).

61. A. Yadav, N. B. Chichkov, E. A. Avrutin, *et al.*, "Edge emitting mode-locked quantum dot lasers," Prog. Quantum Electron. **87**, 100451 (2023).

62. T. Miyajima, H. Watanabe, M. Ikeda, *et al.*, "Picosecond optical pulse generation from self-pulsating bisectional GaN-based blue-violet laser diodes," Appl. Phys. Lett. **94**, 161103 (2009).

63. W. G. Scheibenzuber, U. T. Schwarz, L. Sulmoni, *et al.*, "Bias-dependent absorption coefficient of the absorber section in GaN-based multisection laser diodes," Appl. Phys. Lett. **97**, 181103 (2010).

64. J. Renaudier, R. Brenot, B. Dagens, *et al.*, "45 GHz self-pulsation with narrow linewidth in quantum dot Fabry-Perot semiconductor lasers at 1.5 μm," Electron. Lett. **41**, 1007–1008 (2005).

65. C. Gosset, K. Merghem, A. Martinez, *et al.*, "Subpicosecond pulse generation at 134 GHz using a quantum-dash-based Fabry-Perot laser emitting at 1.56 μm," Appl. Phys. Lett. **88**, 241105 (2006).

66. R. Rosales, K. Merghem, C. Calo, *et al.*, "Optical pulse generation in single section InAs/GaAs quantum dot edge emitting lasers under continuous wave operation," Appl. Phys. Lett. **101**, 221113 (2012).

67. S. Liu, J. C. Norman, D. Jung, *et al.*, "Monolithic 9 GHz passively mode locked quantum dot lasers directly grown on on-axis (001) Si," Appl. Phys. Lett. **113**, 041108 (2018).

68. W. W. Chow, S. Liu, Z. Zhang, *et al.*, "Multimode description of self-mode locking in a single-section quantum-dot laser," Opt. Express **28**, 5317–5330 (2020).

69. F. Grillot, W. W. Chow, B. Dong, *et al.*, "Multimode physics in the mode locking of semiconductor quantum dot lasers," Appl. Sci. **12**, 3504 (2022).

70. H. Souissi, M. Gromovyi, I. Septembre, *et al.*, "Data associated with the article 'Mode-locked waveguide polariton laser'," Recherche Data Gouv (2024), https://doi.org/10.57745/IAU0UK.